Discovery of novel 1,3,8-triazaspiro[4.5]decane derivatives that target the c subunit of F_1/F_O-adenosine triphosphate (ATP) synthase for the treatment of reperfusion damage in myocardial infarction

Giampaolo Morciano [1,2,3,4$], Delia Preti [5$], Gaia Pedriali [2,3,4$], Giorgio Aquila [6], Sonia Missiroli [3,4], Anna Fantinati [5], Natascia Caroccia [3,4], Salvatore Pacifico [5], Massimo Bonora [3,4], Anna Talarico [5], Claudia Morganti [3,4], Paola Rizzo [2,3], Roberto Ferrari [2,3,7], Mariusz R. Wieckowski [8], Gianluca Campo [2,7], Carlotta Giorgi [3,4], Claudio Trapella [4,5*], Paolo Pinton [2,3,4*]

[1] Maria Pia Hospital, GVM Care & Research, 10132, Torino, Italy
[2] Maria Cecilia Hospital, GVM Care & Research, 48033, Cotignola, Ravenna, Italy
[3] Department of Morphology, Surgery and Experimental Medicine, Section of Pathology, Oncology and Experimental Biology, University of Ferrara, 44121, Ferrara, Italy
[4] Laboratory for Technologies of Advanced Therapies (LTTA), University of Ferrara, 44121, Ferrara, Italy
[5] Department of Chemical and Pharmaceutical Sciences, University of Ferrara, 44121, Ferrara, Italy
[6] Department of Medical Sciences, University of Ferrara, 44121, Ferrara, Italy
[7] Cardiovascular Institute, Azienda Ospedaliera-Universitaria S. Anna, 44121, Cona, Ferrara, Italy
[8] Department of Biochemistry, Nencki Institute of Experimental Biology, Polish Academy of Sciences, 02-093, Warsaw, Poland

Abstract

Recent cardiology research studies have reported the role, function and structure of the mitochondrial permeability transition pore (mPTP) and have shown that its opening plays a key role in the progression of myocardial cell death secondary to reperfusion. In this manuscript, we validated a new pharmacological approach as an adjunct to reperfusion in myocardial infarction (MI) treatment and describe the discovery, optimization and structure-activity relationship (SAR) studies of the first small-molecule mPTP opening inhibitors based on a 1,3,8-triazaspiro[4.5]decane scaffold that targets the c subunit of the F_1/F_O-ATP synthase complex. We identified three potential compounds with good mPTP inhibitory activity and beneficial effects in a model of MI, including a decreased apoptotic rate in the whole heart and overall improvement of cardiac function upon administration during reperfusion. The selected compounds did not show off-target effects at the cellular and mitochondrial levels. Moreover, the compounds preserved the mitochondrial ATP content despite interacting with the ATP synthase complex.

Keywords: mPTP/inhibitors/mitochondria/reperfusion damage/apoptosis

Introduction

Programmed cell death (PCD) is a physiological, evolutionarily-conserved event that is essential for both intrauterine and post-embryonic development as well as tissue homeostasis through elimination of damaged cells [1]. In humans, excessive PCD may be the basis of many diseases, including cardiovascular and neurodegenerative disorders. Several types of PCD exist, including mitochondrial permeability transition (MPT)-driven apoptosis [2], during which the inner mitochondrial membrane (IMM), which is typically highly impermeable, exhibits increased permeability with a consequent osmotic influx of solutes in the mitochondrial matrix followed by loss of structural and functional characteristics of the affected mitochondria [3]. This MPT state is considered to be mediated by the mitochondrial permeability transition pore complex (PTPC), a membrane multiprotein platform composed of pore-forming part(s) and modulators that contribute to its conformational state and thus its mechanism of action [4]. Conditions favoring mitochondrial permeability transition pore (mPTP) opening include increased intra-mitochondrial calcium concentrations ($[Ca^{2+}]$), oxidative stress and phosphates as well as high pH levels, all of which occur in ischemia-reperfusion-based injuries [5, 6]. Although many components/modulators of the mPTP have been discovered in recent years [7, 8], the proteins involved in the channel-forming fraction are still under intensive investigation. In two previous studies [9, 10], we provided experimental evidence that the c subunit of F_1/F_O-ATP synthase plays a pivotal role in mPTP activity and mPTP formation, demonstrating a strong correlation between the mPTP functional state and c subunit expression; indeed, depletion of the c subunit reduced channel opening in response to calcium- and oxidative stress-induced stimuli, whereas its overexpression enhanced mPTP opening [9]. Contrary to what was proposed by another study [11], we previously showed that the MPT is linked to the dissociation of F_1/F_O-ATP synthase dimers. Moreover, a proper c-ring conformation is required for MPT induction once F_1/F_O-ATP synthase dimers have dissociated [10]. Other independent groups have confirmed and extended our observations, defining the dissociation of F_1 from F_O during the MPT and recording a leak conductance within the purified c subunit ring that may form the channel of the mPTP [12, 13, 14, 15]. Indeed, major evidence for the so-called "*c-ring hypothesis*" is derived from a comparison between a recent description of a voltage-sensitive pore represented by reconstituted c subunit proteins and lacking cation selectivity [12] and the multi-conductance channel studied in the 80s-90s [16], where c-rings may be exposed during F_1/F_O uncoupling [12]. However, these theories are not entirely

supported by *in silico* simulations [17], and mathematical calculations may not have considered other regulatory proteins that facilitate the channel formation process [14].

While extensive effort has been invested in the synthesis and testing of new mPTP opening inhibitors [18, 19], to the best of our knowledge, none of these inhibitors were designed to target the c subunit expressed in eukaryotic cells or for cardioprotective purposes in the treatment of myocardial infarction (MI); however, Danshensu (DSS), which is isolated from a traditional Chinese herb, is reported to modulate c subunit protein expression and have cell-protective effects [20].

Among ATP synthase inhibitors, oligomycin A was identified in 1958 [21]. Its presence is sensed by a subunit important for the functional and structural coupling between F_O and F_1: the oligomycin sensitivity-conferring protein (OSCP). Recently, an important role of OSCP as a site of interaction with cyclophilin (CyP) D, a matrix protein that can modulate mPTP opening, was discovered. Intriguingly, in the early 2000s, two reports described the potential of oligomycin A to inhibit mPTP opening induced by selenite [22] and its additive effect on cyclosporine A (CsA)-dependent mPTP activity [23]. Therefore, in addition to the finding that oligomycin A binds to the c-ring of yeast mitochondrial ATP synthase as shown in an high-resolution crystal structure model [24], this compound increased the protective effects against MPT conferred by F_1/F_O-ATP synthase, again demonstrating its role in membrane permeability.

With the aim of identifying a new pharmacological approach for the treatment of ischemia-reperfusion-related damage, in this manuscript, we describe the discovery, optimization and structure-activity relationship (SAR) studies of the first small-molecule mPTP inhibitors to target the c subunit of the F_1/F_O-ATP synthase complex. These compounds, which are based on a 1,3,8-triazaspiro[4.5]decane scaffold, may lead to the development of new cardio/neuroprotective agents for the clinical management of ischemic events.

Results

Identification of 1-phenyl-8-tosyl-1,3,8-triazaspiro[4.5]decan-4-one (PP11) as a novel small-molecule inhibitor of the mPTP. Oligomycin A is classified as an mPTP opening inhibitor that targets the c subunit of F_1/F_O-ATP synthase [25]; therefore, it was selected as the reference compound for this project. Indeed, oligomycin A is known to establish several Van der Waals interactions with c subunits, forming a hydrogen bond with Glu [59] through a water molecule bridge through which the carboxyl group of a leucine residue is also recruited

(Figure 1A) [24]. In particular, the southern part of oligomycin A (Figure 1B) is closely engaged by the binding cavity of the c-ring [24]. Considering this information and the need to simplify this natural compound to facilitate easy, accessible synthesis, we explored the activity of a series of small molecules mimicking the southern 1,7-dioxaspiro[5.5]undecane moiety of oligomycin A. To test the hypothesis that the spiro bicyclic fragment may be mandatory for mPTP inhibition, we initially screened a small internal library of spiro derivatives that somewhat resemble the functional structure of the natural compound. These preliminary investigations resulted in the identification of 1-phenyl-1,3,8-triaza-spiro[4,5]decan-4-one derivative **1** (**PP11**, Figure 1C). To assess the efficacy of **PP11** in inhibiting Ca^{2+}-mediated mPTP opening, we first measured its biological activity in HeLa cells by calcein-cobalt assay [26]. mPTP opening was stimulated by the addition of the ionophore ionomycin, and the resulting kinetics were compared. As shown in Figure 1D, the addition of 1 µM ionomycin to cells pretreated with 1 µM **PP11** resulted in desensitization of mPTP opening by approximately 50% as assessed by the slope of the curve after stimulation, which was significantly less than that observed in vehicle-treated cells. Moreover, **PP11** was able to inhibit the mPTP opening in a manner very similar to that of oligomycin A [24, 27, 28] as a direct derivative but at a tenfold lower concentration. These data demonstrated that the small-molecule inhibitor derived from the known compound oligomycin A was able to efficiently inhibit mPTP opening. Therefore, **PP11** was selected as the starting point for further studies.

PP11 accumulates selectively in mitochondria. To monitor and better characterize **PP11**'s biological activity in cells, we investigated its subcellular localization, focusing on the amount localized within mitochondria, the hypothetical site of action. As illustrated in Figure S1A-C, fractionation [29] of living cells treated with vehicle (A) or **PP11** (B) resulted in successful isolation of pure mitochondrial, cytosolic and endoplasmic reticulum (ER) fractions. Samples from each subcellular compartment were analyzed by HPLC-HRMS to detect the compound. As shown in Figure 2C, **PP11** selectively accumulated in the mitochondria without detectable traces in the other subcellular fractions (Figure 2D, E); however, a residual amount of the spiro derivative was detectable in the supernatant fraction (Figure 2F). The same investigation performed after administration of oligomycin A (Figure S1C) revealed a less selective distribution of the compound, with significant amounts detected in all the isolated subcellular compartments (Figure S2).

Moreover, to directly monitor target engagement inside cells, we performed a cellular thermal shift assay (CETSA) [30, 31] using a protocol based on ligand-induced thermal stabilization of the target protein, the c subunit

of F_O-ATP synthase. Thermal shifts at high compound concentrations are known to correlate with median inhibitory concentration (IC_{50}) values and affinities, as measured by other methods [32, 33]; therefore, by using higher concentrations of **PP11**, we were able to detect its binding with the c subunit of F_O-ATP synthase (Figure S1D) between 60-80°C. Despite the low sensitivity of the assay and an inability to perform any molecular docking assays, Figure S1D shows that the c subunit protein was thermally stabilized by **PP11** pretreatment (red-dashed line) and that this effect was absent in other mitochondrial proteins, such as ATP5A (black-dashed line). To further confirm the putative selective **PP11**-c subunit binding, a UPLC-XEVO-TQD (Waters, UK) mass spectrometry investigation of the c subunit protein overexpressed in and immunoprecipitated from isolated mitochondria of **PP11**-pretreated cells was performed. The results from this experiment are reported in Figure S3 and indicate that a significant amount of **PP11** was clearly detectable and bound to the c subunit.

Together, these data confirm the ability of **PP11** to selectively enter mitochondria and bind the c subunit to inhibit mPTP opening.

Design, synthesis and biological characterization of PP11 analogs as inhibitors of the mPTP. Encouraged by the promising biological profile of **PP11** and considering the higher chemical stability of the aza-spiro moiety compared with the spiro-ketal function of oligomycin A, we initiated an SAR investigation of a new bicyclic core to improve compound potency. We applied a versatile synthetic approach that resulted in a series of **PP11** derivatives that were differentially substituted at the N^1 and N^8 positions (Figure 3). We first investigated the effect of replacing the tosyl function at the N^8 position of **PP11** with a benzyl group (compound **6a**) or with different sulfonamide (**8**-**10**), carboxamide (**13, 14**), urea (**15** and **16**) or thiourea (**17**) moieties. The results of the biological assay indicated that the compounds with the benzyl group or (hetero)arylsulfonamide N^8 substitutions exhibited the best performance; these compounds were therefore combined with N^1 phenyl rings at the para/meta positions with both electron donating or withdrawing groups (compounds **6b**-**g**, **11**, **12**). The common synthetic pathway for the preparation of all the investigated final compounds is depicted in Figure 3. α-Aminonitriles **3a-g** were synthesized by a Strecker reaction from the commercially available *N*-benzylpiperidone **2,** which was reacted with (substituted) anilines in the presence of trimethyl silyl cyanide (TMSCN). The nitrile group was then hydrolyzed to the corresponding amide function (**4a**-**g**) by treatment with concentrated sulfuric acid. Spirocyclization was then performed with dimethylformamide dimethyl acetal (DMF-DMA), which resulted in the generation of the unsaturated intermediates **5a-g**. The latter derivatives were

also screened as mPTP inhibitors to evaluate the effect of the C^2-N^3 double bond constraining the 5-membered ring of the bicyclic template. Subsequently, the imidazolinone ring was efficiently reduced with $NaBH_4$ to yield the final compounds **6a**-**g**. Debenzylation at the N^8 position of **6a** and **6b** was performed via hydrogenation under Pd/C catalysis and yielded **7a** and **7b**, respectively, which were employed as key intermediates for the selective functionalization of the N^8 position. Specifically, the sulfonamide derivatives **1** and **8-12** were obtained by treatment of **7a-b** with appropriate sulfonyl chlorides, while N^8 acetylation (**13**) or benzoylation (**14**) was achieved by standard treatment with acetic anhydride or benzoylchloride, respectively. In addition, the urea derivatives **15-16** and the thiourea **17** were prepared from **7a** and the properly substituted isocyanates or isothiocyanates.

To investigate the effectiveness of the new, synthesized **PP11** analogs against mPTP opening, we used the mitochondrial swelling assay as previously described [34]; this protocol is faster than microscopy analysis for the screening of multiple compounds. **PP11** significantly inhibited mPTP opening (Figures 1D and 4B). To demonstrate specificity in measuring Ca^{2+}-induced mPTP opening, we added two positive controls, CsA and ruthenium red (RR), a known mPTP inhibitor and a mitochondrial calcium uptake blocker, respectively. Freshly isolated mouse liver mitochondria were first evaluated to ensure high purity (Figure 4A) and were then stimulated with 500 μM Ca^{2+}, and absorbance at 540 nm, at which a decrease was indicative of swelling, was monitored for 10 minutes (Figure 4B, C). Under these conditions, mitochondria treated with vehicle exhibited marked membrane swelling (red bar), which was significantly prevented by pretreatment with 1 μM CsA and 5 μM RR (green and blue bars, respectively). As shown in Figure 4B, most of the small molecules showed good inhibitory potential compared to the control mitochondrial sample (red bar). In particular, compounds **5c**, **6g** and **10** were significantly more potent than **PP11** in inhibiting mPTP opening. Additional details are shown in panel 4D, including the mean percentages of mPTP inhibition. Figure 4E shows that 1 μM was the lowest dose with the best effectiveness in inhibiting mitochondrial swelling for each selected compound.

Biological profile of the most promising compounds. Overall, mPTP assays revealed a set of three very potent inhibitors (**5c**, **6g** and **10**) with the greatest effects on reducing mitochondrial swelling (Figure 4B) compared to **PP11**.

Given the crucial role of the c subunit in ATP synthase assembly and cellular energy production as a component of the membrane rotor, the basal mitochondrial ATP content and agonist-induced ATP production were

monitored by the luciferin-luciferase assay [35]. Treatment of living cells with 1 μM **PP11** slightly but significantly depleted mitochondrial ATP levels in resting conditions (Figure 5A); similarly, the relative amount of ATP remained low even upon histamine-induced calcium uptake [36] (Figure 5B). The **PP11** derivatives **5c**, **6g** and **10** synthesized with various specific chemical groups, such as electron withdrawing atoms (Cl) or moieties (CF_3) in the aromatic substituents in positions 1 and 8 of the spirodecane scaffold, allowed us to successfully overcome this drawback and step-limiting factor. Indeed, use of the **6g** and **10** inhibitors did not affect ATP levels, but treatment with compound **5c** induced a small decrease in the basal mitochondrial ATP content, which was completely recovered upon Ca^{2+}-induced ATP generation (Figure 5A, B).

To identify possible side effects of the compounds on living cells that may preclude their use in future studies, we evaluated other important mitochondrial parameters. Mitochondrial membrane potential (MMP) and calcium homeostasis are critical factors for the maintenance of physiological functions in cells, including proper respiratory chain function and a wide range of intracellular signaling pathways, respectively. As shown in Figure 5C and D, pretreatment of cells with the **5c**, **6g** and **10** inhibitors did not affect basal MMP or mitochondrial calcium uptake. Moreover, mitochondrial morphology, the number of mitochondria in cells and their network volume were unchanged (Figure 5E).

In addition, the results previously described were further confirmed by the 3-(4,5-Dimethylthiazol-2-yl)-2,5-diphenyltetrazolium bromide (MTT) assay, which showed that treatment of living cells with micromolar concentrations of **5c**, **6g** and **10** for 24 h and 48 h did not induce significant MTT reduction compared with treatment with vehicle (Figure 5F). Only prolonged (72 h) treatment slightly but significantly decreased cell viability *in vitro* (Figure 5F).

The permeability transition pore has been postulated to play an important role in cytochrome c (CytC) release [37]; therefore, we explored the ability of the selected compounds to prevent CytC release from mitochondrial cristae. To correlate mPTP desensitization with apoptotic cell death prevention, we detected the amount of CytC in the cristae of mitochondrial fractions from the mitochondrial swelling assay upon calcium stimulation. Pretreatment with **5c**, **6g** and **10** prevented CytC release as assessed by immunoblot analysis (Figure 5G). Taken together, these findings demonstrated that inhibition of mPTP opening may inhibit CytC release to the cytosol and consequently prevent apoptotic cell death (Figure 6E).

Next, to understand the molecular mechanism by which the selected compounds inhibit mPTP complex activity, we used a previously tested proximity ligation assay (PLA)-based procedure [10] to verify the F_1/F_O-ATP synthase dimerization grade in living cells. Vehicle-treated cells exhibited a considerable amount of red-dotted staining that colocalized with the mitochondrial protein translocase of outer mitochondrial membrane 20 (TOMM20). We showed the F_1/F_O-ATP synthase dimerization status via a PLA intensity profile upon ionomycin administration alone or in the presence of small-molecule inhibitors. As recently published by our lab, the MPT was accompanied by a significant decrease in the PLA signal following 1-µM ionomycin treatment [10]; however, the MPT did not occur with the same intensity in the presence of 1 µM **5c**, **6g** and **10** (Figure 5H). These findings suggest that mPTP desensitization by the synthesized compounds is correlated with stabilization of F_1/F_O-ATP synthase dimers.

Cardioprotective effect of compound 10 in a model of reperfusion injury. Considering the ability of these inhibitors to desensitize mPTP opening (Figure 4B) by stabilizing ATP synthase dimers (Figure 5H) and prevent CytC release (Figure 5G) without affecting long-term cell viability (Figure 5F) and the mitochondrial ATP content (Figure 5A, B), we investigated the effects of compound **10** in an animal model of cardiac reperfusion injury. We isolated beating rat hearts and placed them in a Langendorff system, which was continuously perfused with Krebs-Henseleit buffer (KHB) bubbled with oxygen at 37°C. The *ex vivo* protocol included stabilization of the heart for 20 min, and then, retrograde perfusion was progressively stopped to induce 30 min of global ischemia followed by 1 hour of reperfusion (Figure 6A). After stabilization, the left ventricular developed pressure (LVDP) was 89.8±3 mmHg in the I/R vehicle group. Following reperfusion, the LVDP decreased to 66±5 mmHg, with a mean reduction of 36±9%, indicating successful induction of ischemia (as previously reported [38]). No difference in LVDP was identified among the experimental groups during stabilization. As indicated in panel 6A, compound **10** was administered in the reperfusion phase during the first 10 minutes of reflow. The dose of 10 µM of compound **10** was selected based on previous experiments to identify the highest dose that could be perfused in the heart without toxicity (data not shown). In isolated hearts, perfusion with a constant volume of derivative **10** resulted in decreases in coronary perfusion pressure (CPP) (-17.5±3.4%) and end-diastolic pressure (EDP) (-72±9.86%) (Figure 6B, D) with an increase in LVDP (+36.4±3.9%) (Figure 6C), indicating reduced diastolic stiffness, vasoconstriction and deterioration of myocardial performance, respectively. At the end of the procedure, cell death was analyzed in the hearts by terminal deoxynucleotidyl

transferase dUTP nick-end labeling (TUNEL) assays. In the I/R+vehicle group, 64% of the cardiomyocytes were TUNEL-positive; however, the number of TUNEL-positive cardiomyocytes was significantly reduced in the presence of spiro derivative **10** (Figure 6E).

These findings confirmed the ability of c-ring-targeting agents to inhibit mPTP opening and to protect against cell death in a cardiovascular model.

Discussion and Conclusions

Myocardial infarction is an ischemic heart disease in which mPTP opening is widely accepted as a crucial step in the development of myocardial damage, which is better known as ischemia-reperfusion injury (IRI) [6]. Since up to 50% of the final infarct size is due to IRI, targeting the mPTP complex may be a valuable pharmacological adjunct to reduce infarct size. Currently, although satisfying results have been achieved in *in vitro* and *in vivo* animal models, manipulation of the PTPC and, more generally, mitochondrial targeting do not appear to influence the mortality of affected patients, but they reduce hospital readmission for heart failure [39]. Instead, drugs with a broad-spectrum mechanism of action are currently utilized in clinical practice [39, 40]. The apparent lack of translational value among mitochondrial-targeting drugs can be ascribed first to limited knowledge regarding the exact molecular structure of mPTP; therefore, the appropriate mitochondrial target possibly has not yet been considered. Second, the multifactorial nature of MI should be considered, and the adoption of combined strategies targeting multiple intracellular signaling pathways is always recommended [41].

Based on our previous studies on the role of the c-ring in mPTP opening [9, 10] and to validate a new pharmacological approach for the treatment of ischemia-reperfusion-related damage, in this manuscript, we describe the discovery, optimization and SAR studies of the first small-molecule mPTP opening inhibitors that target the c subunit of the F_1/F_O-ATP synthase complex.

To the best of our knowledge, this is the first attempt to inhibit the mPTP by targeting the eukaryotic c subunit of ATP synthase using novel small molecules for therapeutic purposes. Indeed, treatment during reperfusion with one of the most promising screened compounds (**10**) showed beneficial effects in an *ex vivo* model of MI, with a reduction of apoptotic cell death upon IRI (Figure 6E). The decreases in CPP and EDP (Figure 6B, D) with an increase in LVDP (Figure 6C) in the isolated heart reflected significant reductions in diastolic stiffness, vasoconstriction and deterioration of myocardial performance. Moreover, the *ex vivo* beneficial effects of

compound **10** together with strong inhibition of mPTP opening by the selected compounds *in vitro* can be achieved without altering mitochondrial parameters (Figure 5A-E) or short-term toxicity in living cells. Indeed, these compounds weakly but significantly disrupted cell viability only with 72 h of treatment (Figure 5F).

The compounds were derived using the scaffold of the known c subunit inhibitor oligomycin A; we first identified **PP11**, a compound with a strong desensitization effect on mPTP opening (Figure 1D) and an inhibitory effect comparable to that of oligomycin A, but it is functionally active at a tenfold lower concentration (Figure 1D). The increased performance at lower concentrations can be ascribed to its better localization to the mitochondrial compartment (Figure 2), the putative site of action, as assessed by HPLC-HRMS. Indeed, **PP11** accumulates exclusively in the pure mitochondrial fraction (Figure 2 and Figure S1) without detectable traces in other subcellular compartments. In contrast, although oligomycin A is present in the mitochondrial compartment where it exerts known biological effects, a significant amount diffuses into the cytoplasm and ER organelles (Figure S2), likely lowering its potency and conferring a better drug-like profile to **PP11**. In addition, given its effectiveness in targeting the c subunit for mPTP inhibition [9, 10, 14] and the exclusive mitochondrial localization of its ligand, **PP11** (and derivatives) use led to fewer side effects compared to other known mPTP inhibitors, such as CsA. Indeed, CsA off-target effects [42, 43] are derived from a diffuse intracellular localization pattern characterized by cytosolic [42, 43] and nuclear interactions [44], thus prompting research on alternative methods to target the mPTP.

Criticism could arise from the use of putative ATP synthase disruptors as ligands of the membrane rotor components, as confirmed in this work by the suboptimal effect of **PP11**, a preliminary derivative of oligomycin A, on the mitochondrial ATP content [45]. Indeed, although **PP11** is considered a good mPTP opening inhibitor (Figure 1D), it has a slight deleterious effect on the production of basal ATP (Figure 5A); however, this effect is reduced upon Ca^{2+}-dependent stimulation in the mitochondria (Figure 5B). When designing **PP11** derivatives, we tried to evaluate different chemical modifications at several positions of the parent compound to identify possible structural determinants that can abolish any undesired effects. Among the most promising compounds screened in Figure 4B, **6g** and **10** did not affect the basal mitochondrial ATP content; only compound **5c** promoted a small decrease in the basal mitochondrial ATP content, which was completely recovered upon Ca^{2+}-induced ATP generation. A possible explanation for such experimental evidence may be faster reversibility of the interaction of **6g** and **10** with the postulated cellular target compared to **PP11**.

The main findings of this work are consistent with those of our previously published studies and those of independent groups [12-14, 46], confirming the importance of the roles of i) the c-ring as a core component in mPTP activity and ii) the dimer versus monomer transition of ATP synthase linked to the mPTP and the resulting apoptotic cell death. Indeed, a PLA-dedicated assay suggested dimer stabilization upon Ca^{2+}-triggered mPTP opening when cells were pretreated with the **5c**, **6g** and **10** compounds (Figure 5H) as a molecular mechanism by which these inhibitors may exert anti-apoptotic effects.

We are aware that our data appear to disagree with the hypothesis from Walker JE's group on the persistence of the MPT in a cell clone lacking the c subunit of human ATP synthase [47]; however, as a very exhaustive commentary on this discrepancy explains [48], in the absence of the primary mechanisms in mPTP opening (e.g., c subunit expression), the MPT can presumably occur through other pathways involving misfolded proteins of the mitochondrial membrane [48, 49].

In conclusion, we propose small-molecule c subunit inhibitors as a new pharmacological approach for the treatment of IRI. Future perspectives will be oriented towards the study of ATP synthase conformational changes (if detectable) in terms of modulation of its dynamic assembly into supercomplexes upon inhibitor treatment (for instance, by using native gels) and understanding the exact binding sites between inhibitors and mitochondrial protein(s). Photoaffinity labeling of the most promising compounds identified here may lead to useful tools that will facilitate future binding site deconvolution studies advancing structure-based drug design approaches in this field.

Experimental Section

Chemistry. Reaction progress and product mixtures were monitored by thin-layer chromatography (TLC) on silica gel (precoated F_{254} Macherey-Nagel plates) and visualized with a UV lamp (254-nm light source). The organic solutions from extractions were dried over anhydrous sodium sulfate. Chromatography was performed on Merck 230-400 mesh silica gel or using Isolera One (Biotage Sweden). ^{1}H, ^{13}C, DEPT, bidimensional (gCOSY) and heterocorrelated (gHMQC, gHMBC) NMR spectra were recorded on a VARIAN Mercury Plus 400 MHz spectrometer. Chemical shifts (δ) are reported in parts per million (ppm) using the peak of deuterated solvents as an internal standard, and coupling constants (J) are reported in Hertz. Splitting patterns are designed as s, singlet; d, doublet; t, triplet; q, quartet; m, multiplet; and b, broad. Melting points for purified products were

determined in a glass capillary on a Stuart Scientific electrothermal apparatus SMP3 and are uncorrected. Mass spectra were recorded by an ESI single quadrupole mass spectrometer Waters ZQ 2000 (Waters Instruments UK). For analytical controls, Beckmann System Gold 168 HPLC was used with an LC column Kinetex 5-µm EVO C18 100 Å (250 X 4.6 mm) and a variable wavelength UV detector fixed to 220 nm. The analysis was conducted using two solutions, A and B, containing 100:0.1 H_2O:TFA and 40:60:0.1 H_2O:CH_3CN:TFA, respectively, with a gradient elution of 0-50% solution B over 30 minutes. The purity of all compounds was determined by HPLC and was greater than 95%.

LC-HRMS analysis of crude mitochondria and cytosol of PP11-treated cells and final compounds was performed with an ESI-Q-TOF Nano HPLC-CHIP Cube® Agilent 6520 instrument (Agilent Technologies USA) using a linear gradient (0.4 µL/min) from 0% solvent A (97% water/3% acetonitrile/0.1% formic acid) to 80% solvent B (97% acetonitrile/3% water/0.1% formic acid) over 10 minutes and from 80% to 5% solvent B over 5 minutes using a Zorbax C18 Column (43 mm X 75 µm, 5 µm) equipped with an enrichment column (4 mm, 40 nL). The UPLC-MS analysis was performed in an Acquity UPLC equipped with a triple quadrupole mass spectrometer XEVO-TQD (Waters UK). Chromatographic separation was carried out using a BHE C_{18} column (50 mm X 2.1 mm i.d. 1.8µm) from Waters (Waters, Milford, USA) heated at 40°C. The mobile phase consisted of water with 0.1% formic acid (solvent A) and acetonitrile with 0.1% formic acid (Solvent B). An 8-minute gradient elution at 0.3 mL/min was performed as follows: from 100% solvent A to 80% solvent A over 4 minutes, from 80% A to 20% A over 2 minutes, and from 20% A to 0% A over 2 minutes. Mass spectrometric detection was carried out using an electrospray interface (ESI) operated in positive ionization mode with multiple reaction monitoring (MRM) for the **PP11** analyte. Nitrogen was used as a desolvation gas at a 650-L/h flow rate with the desolvation temperature set at 200°C and the source temperature set at 150°C. The collision gas (argon) flow was set at 0.1 mL/min. The capillary voltage was set at 4 kV; the collision energy and con voltage were optimized to maximize the signal corresponding to the major transition observed in the MS/MS spectra following fragmentation of the $[M+H]^+$ ion corresponding to the **PP11** molecule.

Calcein-cobalt assay. HeLa cells were pretreated with DMSO (vehicle), 10 µM oligomycin A, 1 µM CsA or 1 µM **PP11** and then loaded with calcein acetoxymethyl ester and Co^{2+} as previously described [26]. Staining solution was added to the cells for 15 minutes at 37°C in a 5% CO_2 atmosphere. Image acquisitions were performed with a motorized Olympus IX81-ZDC inverted microscope with a 40×/1.30-N.A. UPlanFLN oil-

immersion objective and Cell MT20E xenon lamp. Ionomycin (1 µM) was administered 30 seconds after the beginning of the experiment to induce mPTP opening.

Mitochondrial isolation and swelling assay. Mitochondria were isolated by conventional procedures involving differential centrifugation. Freshly excised SV129 mouse livers were washed and then homogenized in medium containing 50 mmol/L Tris-HCl, 25.67 g/L sucrose, and 40.98 g/L D-Mannitol (pH 7.4) supplemented with 0.5 mmol/L EGTA and 5 g/L bovine serum albumin (BSA). The homogenate was then transferred to microcentrifuge tubes and centrifuged at 0.8 rcf for 5 minutes for at least 2 cycles; the supernatants were collected, and the pellets were discarded. Subsequently, the sample was centrifuged at 10.0 rcf for 10 minutes to separate the mitochondrial fraction; the pellet was resuspended and ground in a loose-fitting glass Potter Elvehjem homogenizer for a fixed number of times. Samples were then centrifuged at 10.0 rcf for 10 minutes, and the pellet (mitochondria) was resuspended in 1 mL of Respiration Buffer (pH 7.4, Tris-HCl 50 mmol/L; 25.67 g/L sucrose; 40.98 g/L D-Mannitol) supplemented with 5 mmol/L succinate. Mitochondria were quantified and diluted to a final concentration of 1 mg/mL for each mitochondrial swelling assay to monitor the changes in absorbance at 540 nm as previously described [34]. Incubations with small molecules were carried out at 25°C, and mPTP opening was induced by the addition of 500 µM Ca^{2+}.

***Ex vivo* model.** I/R was studied *ex vivo* using the Langendorff model with minor modifications [10]. In brief, upon euthanasia, the hearts of Wistar rats weighing 270-280 g at inclusion into the study were rapidly excised, immediately arrested in ice-cold KHB (pH 7.4; 4°C), cannulated and retrograde perfused at a fixed-flow rate (11 mL/min) through the aorta with warm KHB (37°C) bubbled with 95% O_2 and 5% CO_2. Upon removal of the left atrial appendage, a latex fluid-filled balloon was inserted into the left ventricular chamber through the atrium to obtain an isovolumetrically beating preparation and connected to a pressure transducer (APT300, Hugo-Sachs, Grünstraße, Germany) by a fluid-filled polyethylene catheter to monitor performance. An additional transducer above the aortic cannula monitored the CPP. At the start of each experiment, the fluid in the balloon was increased incrementally to achieve a constant EDP of 4±1 mmHg. The LVDP was then measured. The LVDP, EDP and CPP were continuously recorded using a programmable acquisition system (HSE Isoheart Software for Isolated Heart, Hugo-Sachs, Grünstraße, Germany).

Proximity ligation assays. Cells were fixed in 4% PFA for 10 min at 37°C, washed in PBS, placed in a jar containing 1 mmol/L EDTA buffer (pH 8.0) for 20 min at 100°C (to improve epitope-antibody binding) and

then placed at room temperature for an additional 10 min. Then, the cells were permeabilized with 0.05% Triton X-100 for 10 min at 37°C, and unspecific binding sites were blocked by incubating the cells in 0.05% Triton X-100 supplemented with 2% BSA for 45 min at 37°C. Upon overnight incubation with ATP5H-specific antibodies that were previously conjugated to + or - PLA oligonucleotide probes per the instructions of the Duolink In Situ® Probemaker kits, detection was performed as follows. A ligation-ligase solution was added to each sample for 30 min at 37°C followed by 2 washes for 2 min each with Duolink In Situ® Wash Buffer A; an amplification-polymerase solution was added and incubated for 100 min at 37°C followed by 2 washes for 10 min each with 1x Duolink In Situ® Wash Buffer B and 1 wash for 1 min with 0.01x Duolink In Situ® Wash Buffer B. Cells were fixed again in 4% PFA for 10 min at 37°C and then blocked in 0.05% Triton X-100 supplemented with 2% BSA for 10 min at 37°C. Finally, the samples were incubated overnight with primary anti-TOM20 antibody, and the next day, the primary antibodies were revealed by incubation with the appropriate goat anti-rabbit Alexa Fluor 488® secondary antibodies. The slides were then stained with Duolink In Situ® Detection Reagent Red and mounted using DAPI-containing Duolink In Situ® Mounting Medium. Protein proximity was evaluated on an Axiovert 200M fluorescence microscope equipped with a 40X water immersion objective (N.A. 1.2, from Carl Zeiss Microscopy, LLC) as a function of mitochondrial-localized red signal intensity.

Statistical analysis. The statistical method included one-way ANOVA with multiple comparisons performed by GraphPad Prism. P values are reported in the figure legends.

ASSOCIATED CONTENTS

Supporting Information

Supplementary Methods; General procedures for the preparation of compounds **3a-g**, **4a-g**, **5a-g**, **6a-g**, **7a-b**, **1** and **8-17**; ^{1}H, ^{13}C, DEPT NMR spectra of compounds **1**, **8-17**, and **6a-g**; HRMS spectra of compounds **5a-g**, **6a-g**, **1**, and **8-17**; Figures S1, S2 and S3 (.PDF)

Molecular formula strings for the final compounds **5a-g**, **1**, **8-17** (.CSV).

AUTHOR INFORMATION

Corresponding Authors

*Paolo Pinton

Email: paolo.pinton@unife.it

*Claudio Trapella

Email: claudio.trapella@unife.it

Author Contributions

$ G.M., D.P. and G.P. equally contributed to this manuscript.

ACKNOWLEDGMENTS

PP is grateful to Camilla degli Scrovegni for continuous support. PP is supported by the Italian Ministry of Education, University and Research, the Italian Ministry of Health, Telethon (GGP15219/B), the Italian Association for Cancer Research (AIRC: IG-18624), and by local funds from the University of Ferrara. CG is supported by local funds from the University of Ferrara, the Italian Association for Cancer Research (AIRC: IG-19803), the Italian Ministry of Health, and by a Fondazione Cariplo grant. GM would like to acknowledge Pierangelo M. for his support. GM is supported by a grant within Bayer's initiative "Grants4Targets". DP is supported by the fund FIR (Fondo per l'Incentivazione alla Ricerca) of the University of Ferrara (Year: 2016; code: FIR1679708). MRW is supported by the Polish National Science Centre (UMO-2014/15/B/NZ1/00490).

ABBREVIATIONS USED

CETSA: cellular thermal shift assay, CsA: cyclosporine A, CPP: coronary perfusion pressure, CytC: cytochrome c, EDP: end-diastolic pressure, IMM: inner mitochondrial membrane, KRB: Krebs-Henseleit buffer, LVDP: left ventricular developed pressure, MI: myocardial infarction, MMP: mitochondrial membrane potential, MPT: mitochondrial permeability transition, PCD: programmed cell death, PLA: proximity ligation assay, PTPC: permeability transition pore complex, RR: ruthenium red, SAR: structure-activity relationship, TUNEL: terminal deoxynucleotidyl transferase dUTP nick-end labeling.

Conflict of interest: The authors declare no competing financial interest.

References

1. Meier, P.; Finch, A.; Evan, G. Apoptosis in development. *Nature* **2000,** *407*, 796-801.

2. Izzo, V.; Bravo-San Pedro, J. M.; Sica, V.; Kroemer, G.; Galluzzi, L. Mitochondrial permeability transition: new findings and persisting uncertainties. *Trends Cell Biol* **2016,** *26*, 655-667.

3. Bonora, M.; Wieckowsk, M. R.; Chinopoulos, C.; Kepp, O.; Kroemer, G.; Galluzzi, L.; Pinton, P. Molecular mechanisms of cell death: central implication of ATP synthase in mitochondrial permeability transition. *Oncogene* **2015,** *34*, 1608.

4. Halestrap, A. P. A pore way to die: the role of mitochondria in reperfusion injury and cardioprotection. *Biochem Soc Trans* **2010,** *38*, 841-860.

5. Morciano, G.; Giorgi, C.; Bonora, M.; Punzetti, S.; Pavasini, R.; Wieckowski, M. R.; Campo, G.; Pinton, P. Molecular identity of the mitochondrial permeability transition pore and its role in ischemia-reperfusion injury. *J Mol Cell Cardiol* **2015,** *78*, 142-153.

6. Ferrari, R.; Balla, C.; Malagu, M.; Guardigli, G.; Morciano, G.; Bertini, M.; Biscaglia, S.; Campo, G. Reperfusion damage - a story of success, failure, and hope. *Circ J* **2017,** *81*, 131-141.

7. Giorgio, V.; Bisetto, E.; Soriano, M. E.; Dabbeni-Sala, F.; Basso, E.; Petronilli, V.; Forte, M. A.; Bernardi, P.; Lippe, G. Cyclophilin D modulates mitochondrial F0F1-ATP synthase by interacting with the lateral stalk of the complex. *J Biol Chem* **2009,** *284*, 33982-33988.

8. Shanmughapriya, S.; Rajan, S.; Hoffman, N. E.; Higgins, A. M.; Tomar, D.; Nemani, N.; Hines, K. J.; Smith, D. J.; Eguchi, A.; Vallem, S.; Shaikh, F.; Cheung, M.; Leonard, N. J.; Stolakis, R. S.; Wolfers, M. P.; Ibetti, J.; Chuprun, J. K.; Jog, N. R.; Houser, S. R.; Koch, W. J.; Elrod, J. W.; Madesh, M. SPG7 is an essential and conserved component of the mitochondrial permeability transition pore. *Mol Cell* **2015,** *60*, 47-62.

9. Bonora, M.; Bononi, A.; De Marchi, E.; Giorgi, C.; Lebiedzinska, M.; Marchi, S.; Patergnani, S.; Rimessi, A.; Suski, J. M.; Wojtala, A.; Wieckowski, M. R.; Kroemer, G.; Galluzzi, L.; Pinton, P. Role of the c subunit of the FO ATP synthase in mitochondrial permeability transition. *Cell Cycle* **2013,** *12*, 674-683.

10. Bonora, M.; Morganti, C.; Morciano, G.; Pedriali, G.; Lebiedzinska-Arciszewska, M.; Aquila, G.; Giorgi, C.; Rizzo, P.; Campo, G.; Ferrari, R.; Kroemer, G.; Wieckowski, M. R.; Galluzzi, L.; Pinton, P. Mitochondrial permeability transition involves dissociation of F1FO ATP synthase dimers and C-ring conformation. *EMBO Rep* **2017,** *18*, 1077-1089.

11. Giorgio, V.; von Stockum, S.; Antoniel, M.; Fabbro, A.; Fogolari, F.; Forte, M.; Glick, G. D.; Petronilli, V.; Zoratti, M.; Szabo, I.; Lippe, G.; Bernardi, P. Dimers of mitochondrial ATP synthase form the permeability transition pore. *Proc Natl Acad Sci U S A* **2013,** *110*, 5887-5892.

12. Alavian, K. N.; Beutner, G.; Lazrove, E.; Sacchetti, S.; Park, H. A.; Licznerski, P.; Li, H.; Nabili, P.; Hockensmith, K.; Graham, M.; Porter, G. A., Jr.; Jonas, E. A. An uncoupling channel within the c-subunit ring of the F1FO ATP synthase is the mitochondrial permeability transition pore. *Proc Natl Acad Sci U S A* **2014,** *111*, 10580-10585.

13. Azarashvili, T.; Odinokova, I.; Bakunts, A.; Ternovsky, V.; Krestinina, O.; Tyynela, J.; Saris, N. E. Potential role of subunit c of F0F1-ATPase and subunit c of storage body in the mitochondrial permeability transition. Effect of the phosphorylation status of subunit c on pore opening. *Cell Calcium* **2014,** *55*, 69-77.

14. Elustondo, P. A.; Nichols, M.; Negoda, A.; Thirumaran, A.; Zakharian, E.; Robertson, G. S.; Pavlov, E. V. Mitochondrial permeability transition pore induction is linked to formation of the complex of ATPase C-subunit, polyhydroxybutyrate and inorganic polyphosphate. *Cell Death Discov* **2016,** *2*, 16070.

15. Morciano, G.; Bonora, M.; Giorgi, C.; Pinton, P. Other bricks for the correct construction of the mitochondrial permeability transition pore complex. *Cell Death Dis* **2017,** *8*, e2698.

16. Zorov, D. B.; Kinnally, K. W.; Perini, S.; Tedeschi, H. Multiple conductance levels in rat heart inner mitochondrial membranes studied by patch clamping. *Biochim Biophys Acta* **1992,** *1105*, 263-270.

17. Zhou, W.; Marinelli, F.; Nief, C.; Faraldo-Gomez, J. D. Atomistic simulations indicate the c-subunit ring of the F1Fo ATP synthase is not the mitochondrial permeability transition pore. *Elife* **2017,** *6.*

18. Fancelli, D.; Abate, A.; Amici, R.; Bernardi, P.; Ballarini, M.; Cappa, A.; Carenzi, G.; Colombo, A.; Contursi, C.; Di Lisa, F.; Dondio, G.; Gagliardi, S.; Milanesi, E.; Minucci, S.; Pain, G.; Pelicci, P. G.; Saccani, A.; Storto, M.; Thaler, F.; Varasi, M.; Villa, M.; Plyte, S. Cinnamic anilides as new mitochondrial permeability transition pore inhibitors endowed with ischemia-reperfusion injury protective effect in vivo. *J Med Chem* **2014,** *57*, 5333-5347.

19. Martin, L. J.; Fancelli, D.; Wong, M.; Niedzwiecki, M.; Ballarini, M.; Plyte, S.; Chang, Q. GNX-4728, a novel small molecule drug inhibitor of mitochondrial permeability transition, is therapeutic in a mouse model of amyotrophic lateral sclerosis. *Front Cell Neurosci* **2014,** *8*, 433.

20. Yin, Y.; Guan, Y.; Duan, J.; Wei, G.; Zhu, Y.; Quan, W.; Guo, C.; Zhou, D.; Wang, Y.; Xi, M.; Wen, A. Cardioprotective effect of Danshensu against myocardial ischemia/reperfusion injury and inhibits apoptosis of H9c2 cardiomyocytes via Akt and ERK1/2 phosphorylation. *Eur J Pharmacol* **2013,** *699*, 219-226.

21. Lardy, H. A.; Johnson, D.; Mc, M. W. Antibiotics as tools for metabolic studies. I. A survey of toxic antibiotics in respiratory, phosphorylative and glycolytic systems. *Arch Biochem Biophys* **1958,** *78*, 587-597.

22. Zhu, Y.; Xu, H.; Huang, K. Mitochondrial permeability transition and cytochrome c release induced by selenite. *J Inorg Biochem* **2002,** *90*, 43-50.

23. Chavez, E.; Rodriguez, J. S.; Garcia, G.; Garcia, N.; Correa, F. Oligomycin strengthens the effect of cyclosporin A on mitochondrial permeability transition by inducing phosphate uptake. *Cell Biol Int* **2005,** *29*, 551-558.

24. Symersky, J.; Osowski, D.; Walters, D. E.; Mueller, D. M. Oligomycin frames a common drug-binding site in the ATP synthase. *Proc Natl Acad Sci U S A* **2012,** *109*, 13961-13965.

25. Hong, S.; Pedersen, P. L. ATP synthase and the actions of inhibitors utilized to study its roles in human health, disease, and other scientific areas. *Microbiol Mol Biol Rev* **2008,** *72*, 590-641.

26. Bonora, M.; Morganti, C.; Morciano, G.; Giorgi, C.; Wieckowski, M. R.; Pinton, P. Comprehensive analysis of mitochondrial permeability transition pore activity in living cells using fluorescence-imaging-based techniques. *Nat Protoc* **2016,** *11*, 1067-1080.

27. Chinopoulos, C.; Szabadkai, G. What makes you can also break you: mitochondrial permeability transition pore formation by the c subunit of the F(1)F(0) ATP-synthase? *Front Oncol* **2013,** *3*, 25.

28. Blanchet, L.; Grefte, S.; Smeitink, J. A.; Willems, P. H.; Koopman, W. J. Photo-induction and automated quantification of reversible mitochondrial permeability transition pore opening in primary mouse myotubes. *PLoS One* **2014,** *9*, e114090.

29. Suski, J. M.; Lebiedzinska, M.; Wojtala, A.; Duszynski, J.; Giorgi, C.; Pinton, P.; Wieckowski, M. R. Isolation of plasma membrane-associated membranes from rat liver. *Nat Protoc* **2014,** *9*, 312-322.

30. Jafari, R.; Almqvist, H.; Axelsson, H.; Ignatushchenko, M.; Lundback, T.; Nordlund, P.; Martinez Molina, D. The cellular thermal shift assay for evaluating drug target interactions in cells. *Nat Protoc* **2014,** *9*, 2100-2122.

31. Martinez Molina, D.; Jafari, R.; Ignatushchenko, M.; Seki, T.; Larsson, E. A.; Dan, C.; Sreekumar, L.; Cao, Y.; Nordlund, P. Monitoring drug target engagement in cells and tissues using the cellular thermal shift assay. *Science* **2013,** *341*, 84-87.

32. Fedorov, O.; Marsden, B.; Pogacic, V.; Rellos, P.; Muller, S.; Bullock, A. N.; Schwaller, J.; Sundstrom, M.; Knapp, S. A systematic interaction map of validated kinase inhibitors with Ser/Thr kinases. *Proc Natl Acad Sci U S A* **2007,** *104*, 20523-20528.

33. Wahlberg, E.; Karlberg, T.; Kouznetsova, E.; Markova, N.; Macchiarulo, A.; Thorsell, A. G.; Pol, E.; Frostell, A.; Ekblad, T.; Oncu, D.; Kull, B.; Robertson, G. M.; Pellicciari, R.; Schuler, H.; Weigelt, J. Family-wide chemical profiling and structural analysis of PARP and tankyrase inhibitors. *Nat Biotechnol* **2012,** *30*, 283-288.

34. Di Lisa, F.; Menabo, R.; Canton, M.; Barile, M.; Bernardi, P. Opening of the mitochondrial permeability transition pore causes depletion of mitochondrial and cytosolic NAD+ and is a causative event in the death of myocytes in postischemic reperfusion of the heart. *J Biol Chem* **2001,** *276*, 2571-2575.

35. Morciano, G.; Sarti, A. C.; Marchi, S.; Missiroli, S.; Falzoni, S.; Raffaghello, L.; Pistoia, V.; Giorgi, C.; Di Virgilio, F.; Pinton, P. Use of luciferase probes to measure ATP in living cells and animals. *Nat Protoc* **2017,** *12*, 1542-1562.

36. Jouaville, L. S.; Pinton, P.; Bastianutto, C.; Rutter, G. A.; Rizzuto, R. Regulation of mitochondrial ATP synthesis by calcium: evidence for a long-term metabolic priming. *Proc Natl Acad Sci U S A* **1999,** *96*, 13807-13812.

37. Baines, C. P.; Kaiser, R. A.; Purcell, N. H.; Blair, N. S.; Osinska, H.; Hambleton, M. A.; Brunskill, E. W.; Sayen, M. R.; Gottlieb, R. A.; Dorn, G. W.; Robbins, J.; Molkentin, J. D. Loss of cyclophilin D reveals a critical role for mitochondrial permeability transition in cell death. *Nature* **2005,** *434*, 658-662.

38. Bell, R. M.; Mocanu, M. M.; Yellon, D. M. Retrograde heart perfusion: the Langendorff technique of isolated heart perfusion. *J Mol Cell Cardiol* **2011,** *50*, 940-950.

39. Campo, G.; Pavasini, R.; Morciano, G.; Lincoff, A. M.; Gibson, C. M.; Kitakaze, M.; Lonborg, J.; Ahluwalia, A.; Ishii, H.; Frenneaux, M.; Ovize, M.; Galvani, M.; Atar, D.; Ibanez, B.; Cerisano, G.; Biscaglia, S.; Neil, B. J.; Asakura, M.; Engstrom, T.; Jones, D. A.; Dawson, D.; Ferrari, R.; Pinton, P.; Ottani, F. Clinical

benefit of drugs targeting mitochondrial function as an adjunct to reperfusion in ST-segment elevation myocardial infarction: A meta-analysis of randomized clinical trials. *Int J Cardiol* **2017,** *244*, 59-66.

40. Campo, G.; Pavasini, R.; Morciano, G.; Lincoff, M. A.; M, C. G.; Kitakaze, M.; Lonborg, J.; Ahluwalia, A.; Ishii, H.; Frenneaux, M.; Ovize, M.; Galvani, M.; Atar, D.; Ibanez, B.; Cerisano, G.; Biscaglia, S.; Neil, B. J.; Asakura, M.; Engstrom, T.; Jones, D. A.; Dawson, D.; Ferrari, R.; Pinton, P.; Ottani, F. Data on administration of cyclosporine, nicorandil, metoprolol on reperfusion related outcomes in ST-segment elevation myocardial infarction treated with percutaneous coronary intervention. *Data Brief* **2017,** *14*, 197-205.

41. Hausenloy, D. J.; Yellon, D. M. Combination therapy to target reperfusion injury after ST-segment-elevation myocardial infarction: a more effective approach to cardioprotection. *Circulation* **2017,** 136, 904-906.

42. Abikhair, M.; Mitsui, H.; Yanofsky, V.; Roudiani, N.; Ovits, C.; Bryan, T.; Oberyszyn, T. M.; Tober, K. L.; Gonzalez, J.; Krueger, J. G.; Felsen, D.; Carucci, J. A. Cyclosporine A immunosuppression drives catastrophic squamous cell carcinoma through IL-22. *JCI Insight* **2016,** *1*, e86434.

43. Youn, T. J.; Piao, H.; Kwon, J. S.; Choi, S. Y.; Kim, H. S.; Park, D. G.; Kim, D. W.; Kim, Y. G.; Cho, M. C. Effects of the calcineurin dependent signaling pathway inhibition by cyclosporin A on early and late cardiac remodeling following myocardial infarction. *Eur J Heart Fail* **2002,** *4*, 713-718.

44. Le Hir, M.; Su, Q.; Weber, L.; Woerly, G.; Granelli-Piperno, A.; Ryffel, B. In situ detection of cyclosporin A: evidence for nuclear localization of cyclosporine and cyclophilins. *Lab Invest* **1995,** *73*, 727-733.

45. Matsuno-Yagi, A.; Hatefi, Y. Kinetic modalities of ATP synthesis. Regulation by the mitochondrial respiratory chain. *J Biol Chem* **1986,** *261*, 14031-14038.

46. Beutner, G.; Alanzalon, R. E.; Porter, G. A., Jr. Cyclophilin D regulates the dynamic assembly of mitochondrial ATP synthase into synthasomes. *Sci Rep* **2017,** *7*, 14488.

47. He, J.; Ford, H. C.; Carroll, J.; Ding, S.; Fearnley, I. M.; Walker, J. E. Persistence of the mitochondrial permeability transition in the absence of subunit c of human ATP synthase. *Proc Natl Acad Sci U S A* **2017,** *114*, 3409-3414.

48. Amodeo, G. F.; Torregrosa, M. E. S.; Pavlov, E. V. From ATP synthase dimers to C-ring conformational changes: unified model of the mitochondrial permeability transition pore. *Cell Death Dis* **2017,** *8,* 1.

49. He, L.; Lemasters, J. J. Regulated and unregulated mitochondrial permeability transition pores: a new paradigm of pore structure and function? *FEBS Lett* **2002,** *512,* 1-7.

Figure legends

Figure 1. Discovery of PP11 as the first small-molecule inhibitor of the mPTP with a spirocenter template that mimics the spiroketal moiety of oligomycin A.

A: Graphical representation of the key amino acid residues defining the binding pocket of the known mPTP inhibitor oligomycin A to the c-ring.

B: Structure of the southern portion of oligomycin A showing a 1,7-dioxaspiro[5.5]undecan moiety that is closely involved in the interaction with the c-ring.

C: Structure of PP11, a novel small-molecule inhibitor of the mPTP with a 1,3,8-triaza-spiro[4.5]decan-4-one template.

D: Calcein-cobalt assay in living cells pretreated with vehicle, oligomycin A, PP11 and CsA. mPTP opening was stimulated by ionomycin administration, and representative kinetics data are reported.

***: p value<0.001; ****: p value<0.0001. CsA: cyclosporine A.

Figure 2. PP11 selectively localizes in mitochondria.

Subcellular localization of **PP11** was investigated via HPLC-HRMS analysis of samples from different cellular compartments before and after treatment with the compound.

A: The HPLC-HRMS profile of **PP11** analyzed in physiological solution revealed broad band absorption (7-8.5 min) with maximum absorption at a retention time of 8.03 min (top panel). The blue region of the HPLC spectrum corresponds to a unique mass peak at $[M+H]^+$ *m/z* of 386.15339 (bottom panel, $[M+H]^+$ calculated for **PP11** 386.1533).

B: The HPLC profile of the mitochondrial fraction isolated from untreated cells revealed a relatively clean zone in the detection region of **PP11** (from 7 to 8.5 min, top panel). The gray band on the HPLC spectrum corresponds to the mass spectra area between the retention time of 7 to 8.5 minutes enlarged in the bottom panel.

C: The HPLC-HRMS profile of the mitochondrial fraction isolated from cells pretreated with **PP11** clearly indicated the presence of the **PP11** compound with an HPLC band at a retention time of 8.2 min (top panel). The red area of the signal corresponds to the enlarged TIC signal for the mass peaks (bottom panel), among which the $[M+H]^+$ *m/z* of 386.15339 indicated that the presence of **PP11** was not detectable in the corresponding untreated fraction (panel B).

D: No detectable amount of **PP11** was found by HPLC-HRMS in the cytosolic fraction of **PP11**-treated cells.

E: The HPLC profile of the ER fraction isolated from **PP11**-treated cells revealed a relatively clean zone in the detection region of **PP11** (from 7 to 8.5 min, top panel). The gray band of the HPLC spectrum corresponds to enlargement of the TIC signals of mass peaks detected by HRMS analysis (bottom panel).

F: The HPLC-HRMS profile of the supernatant fraction isolated from cells pretreated with **PP11** indicated the presence of the compound.

Figure 3. Synthesis of PP11 and related spiro bicyclic derivatives.

Figure 4. Screening of PP11 analogs.

A: Immunoblot detection of GAPDH (cytosolic marker) and TIM23 (mitochondrial marker) proteins in the homogenate (H) of the whole liver and in the mitochondrial (Mito) fraction.

B: Mitochondrial swelling assay for the screening of compounds in freshly isolated mouse liver mitochondria. Data were obtained by recording changes in absorbance (540 nm), and then, the data were converted into percentages. Black bar: untreated and unstimulated mitochondria; red bar: untreated mitochondria stimulated with 500 µM Ca^{2+}; green bar: pretreatment with 1 µM CsA and stimulation with 500 µM Ca^{2+}; blue bar: pretreatment with 5 µM RR and stimulation with 500 µM Ca^{2+}; cyan bar: pretreatment with 1 µM **PP11** and stimulation with 500 µM Ca^{2+}; and white bars: pretreatment with 1 µM **PP11** analogs and stimulation with 500 µM Ca^{2+}. Red arrows indicate the three selected compounds.

C: Kinetics and statistical data from the mitochondrial swelling assay for the vehicle, CsA, RR, **5c**, **6g** and **10** experimental conditions.

D: Mean percentages of mPTP inhibition with the tested compounds.

E: Dose-responses for the **5c**, **6g** and **10** compounds.

One-way ANOVA was used for statistical analysis; *: p value<0.05; **: p value<0.01; CsA: cyclosporine A; RR: ruthenium red.

Figure 5. Biological profile of the most promising compounds.

A: Mitochondrial ATP content in living cells at resting conditions using the luciferase-luciferin method.

B: Mitochondrial ATP generation upon agonist-induced Ca^{2+} uptake in living cells using the luciferase-luciferin method. His indicates 100 µM histamine, the agonist used to induce Ca^{2+}-dependent ATP production.

C: TMRM fluorescence as an index of mitochondrial membrane potential changes in living cells.

D: Mitochondrial calcium uptake in living cells using a mitochondrially-targeted aequorin probe; histograms of statistical and representative kinetics data; 100 µM histamine (His) addition is indicated.

E: Evaluation of mitochondrial morphology parameters using an mtCHERRY probe.

F: MTT assay in living cells to evaluate the toxicity of compounds at 24 h, 48 h and 72 h and at different concentrations. Black bar: cells treated with vehicle; and green bar: 1 µM compound; yellow bar: 5 µM; red bar: 10 µM. The data were standardized to the vehicle condition.

G: Immunoblot detection of cytochrome c in both mitochondrial cristae and respiration buffer from the mitochondrial swelling assay. HSP60 was used as a mitochondrial marker, and GAPDH was used as a cytosolic marker.

H: PLA-based assay for assessment of the ATP synthase dimerization status. Blue: nuclei by DAPI detection; green: mitochondria by TOM20 detection; red spots: ATP5H detection as described in the methods. Representative images are shown below.

a.u.: arbitrary units; CytC: cytochrome c; n.s: not significant; *: p value<0.05; **: p value<0.01; and ****: p value<0.0001; IB: immunoblotting.

Figure 6. Beneficial effects of compound 10 in a cardiac reperfusion injury model.

A: Diagram depicting the standard Langendorff *ex vivo* protocol.

B: Coronary perfusion pressure recording of a rat heart in the stabilization, ischemia and reperfusion phases. Compound **10** is used at a concentration of 10 µM.

C: Left ventricular peak developed pressure recording of a rat heart in the stabilization, ischemia and reperfusion phases.

D: End-diastolic pressure recording of a rat heart in the stabilization, ischemia and reperfusion phases.

E: TUNEL assay for apoptosis evaluation under experimental conditions and representative images. Red: nuclei detected by TO-PRO; green: apoptotic nuclei detected by TUNEL enzyme.

**: p value<0.01; and ****: p value<0.0001. The green bar in panels A-D indicates vehicle or compound administration time.

Figure 1

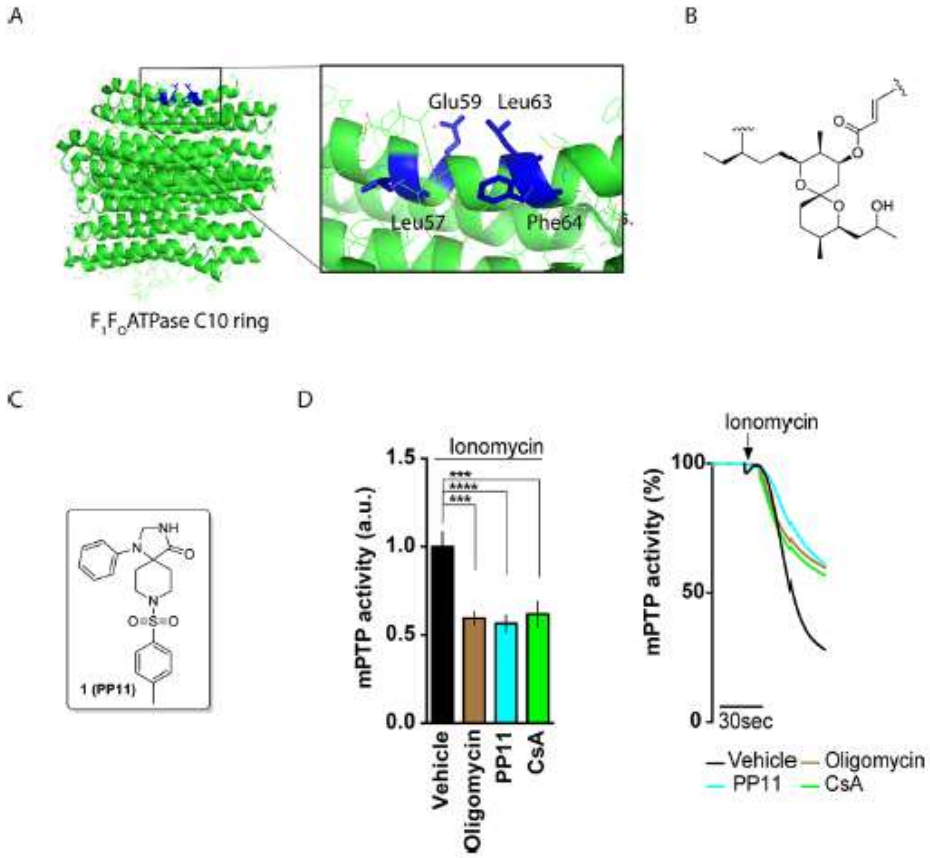
A
Glu59
Leu63
Leu57
Phe64
F1FOATPase C10 ring
B
OH
C
NH
1 (PP11)
D
Ionomycin
mPTP activity (a.u.)
1.5
1.0
0.5
0.0
Vehicle
Oligomycin
PP11
CsA
Ionomycin
mPTP activity (%)
100
50
0
30sec
Vehicle
Oligomycin
PP11
CsA

Figure 2

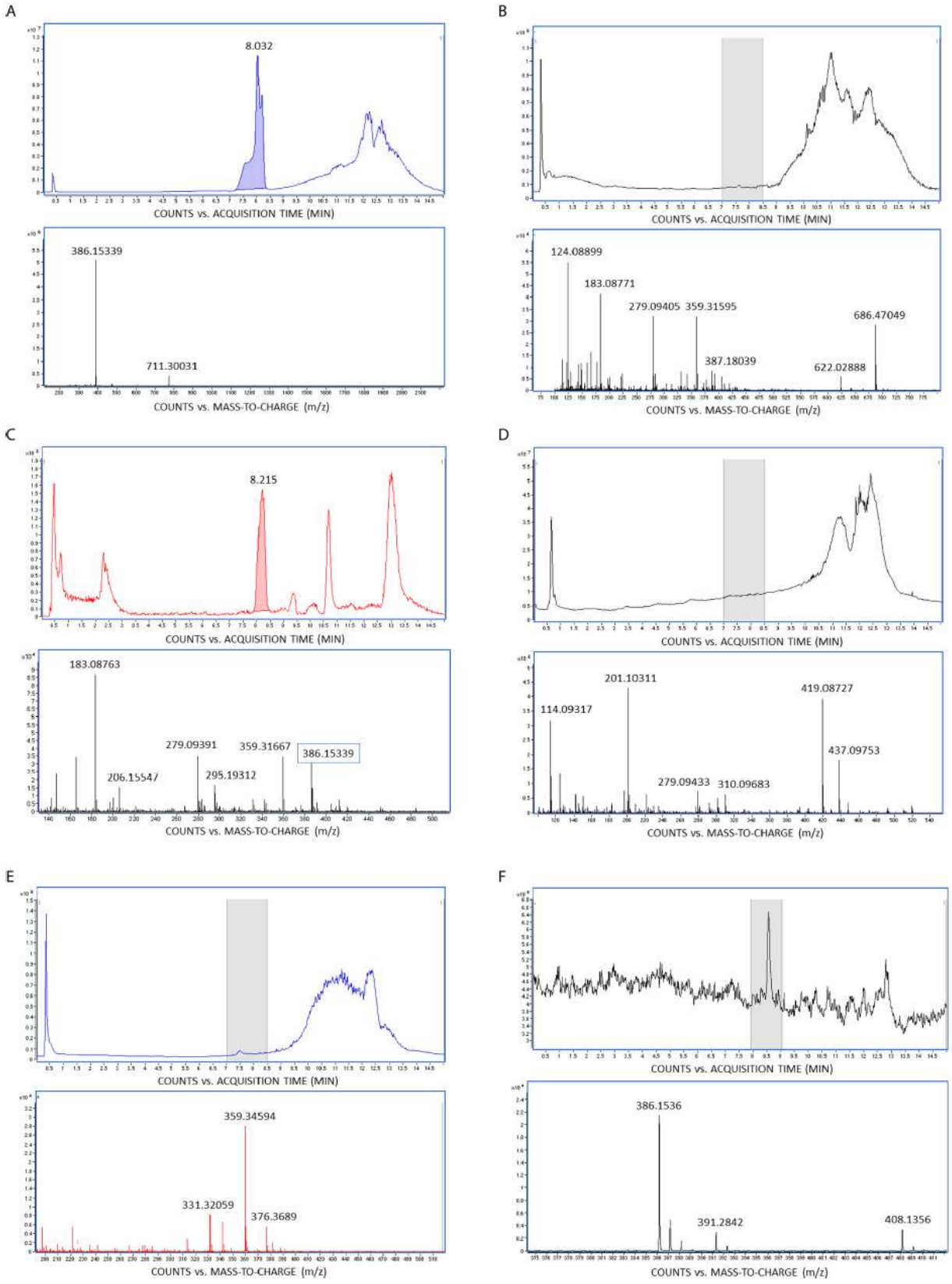
A
8.032
COUNTS vs. ACQUISITION TIME (MIN)
386.15339
711.30031
COUNTS vs. MASS-TO-CHARGE (m/z)
B
COUNTS vs. ACQUISITION TIME (MIN)
124.08899
183.08771
279.09405
359.31595
686.47049
387.18039
622.02888
COUNTS vs. MASS-TO-CHARGE (m/z)
C
8.215
COUNTS vs. ACQUISITION TIME (MIN)
183.08763
279.09391
359.31667
386.15339
206.15547
295.19312
COUNTS vs. MASS-TO-CHARGE (m/z)
D
COUNTS vs. ACQUISITION TIME (MIN)
201.10311
419.08727
114.09317
437.09753
279.09433
310.09683
COUNTS vs. MASS-TO-CHARGE (m/z)
E
COUNTS vs. ACQUISITION TIME (MIN)
359.34594
331.32059
376.3689
COUNTS vs. MASS-TO-CHARGE (m/z)
F
COUNTS vs. ACQUISITION TIME (MIN)
386.1536
391.2842
408.1356
COUNTS vs. MASS-TO-CHARGE (m/z)

Figure 3

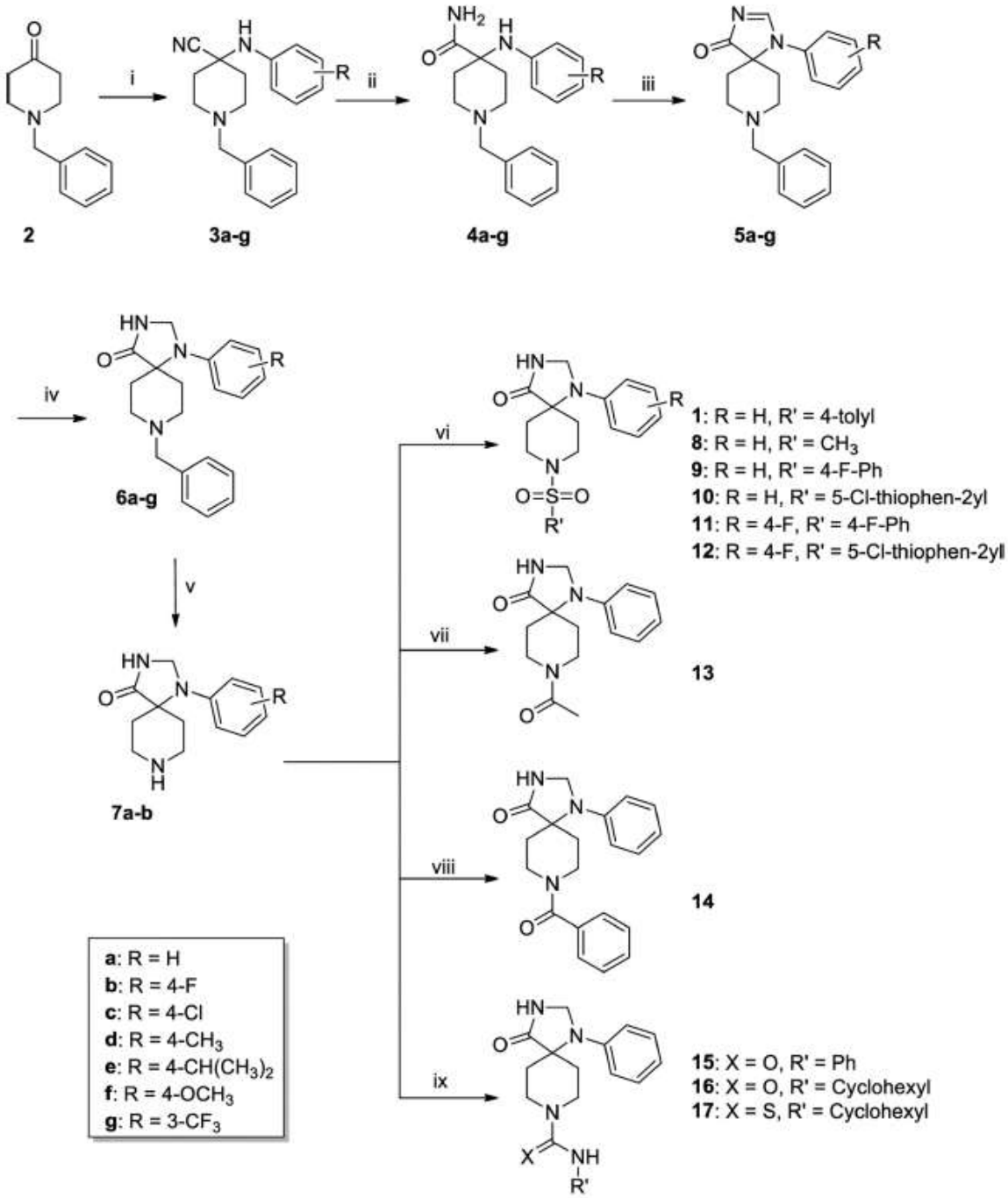

Reagents and conditions:

i) Substituted anilines, TMSCN, AcOH, rt, 2.5 h
ii) H_2SO_4, rt, 18 h
iii) DMF-DMA, MeOH, 55°C, 16 h
iv) $NaBH_4$, MeOH, rt, 2 h
v) H_2, 10% C/Pd, MeOH, CH_3COOH, 16 h
vi) $R'SO_2Cl$, DIPEA, THF, rt, 2 h
vii) Ac_2O, TEA, DCM, rt, 16 h
viii) BzCl, TEA, DCM, rt, 2 h
ix) R'N=C=X, TEA,1,2-DCE, rt or reflux, 1-16 h

Figure 4

A

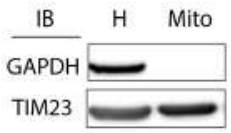

B

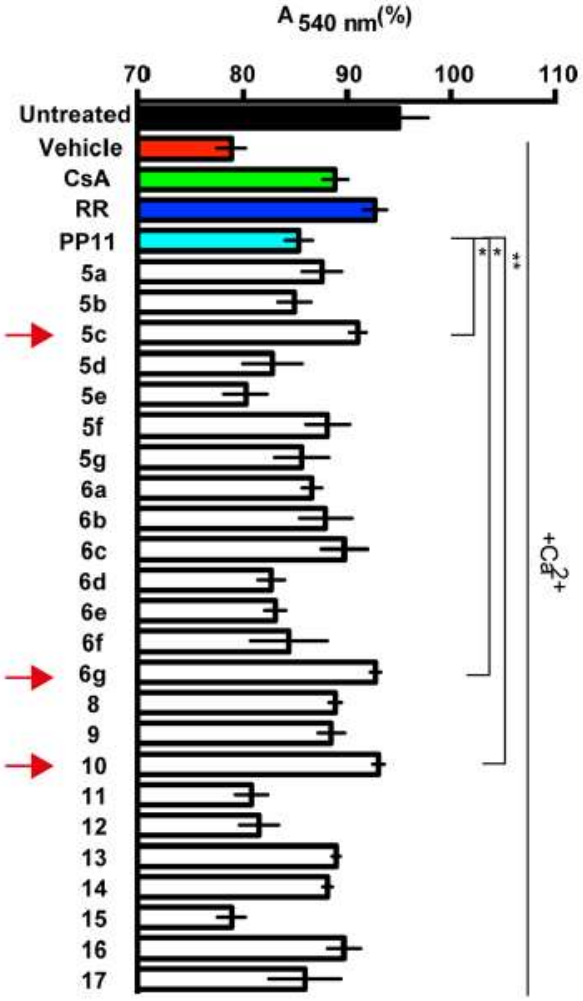

C

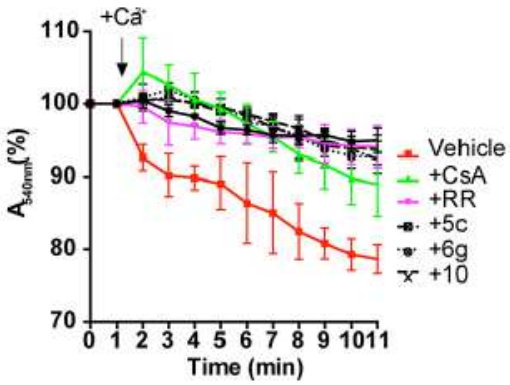

D

Compound	mPTP inhibition (%)
N^{δ}-benzyl derivatives	
5a	41,4
5b	28,8
5c	57,4
5d	18,7
5e	6,5
5f	43,8
5g	32,1
6a	36,8
6b	42,9
6c	51,4
6d	18,1
6e	20
6f	26,2
6g	65,5
N^{δ}-sulfonamide derivatives	
1 (PP11)	30,7
8	47,5
9	45,5
10	66,8
11	9,1
12	12,6
N^{δ}-carboxamide derivatives	
13	47,9
14	43,9
N^{δ}-(thio)urea derivatives	
15	None
16	51,3
17	33,6

E

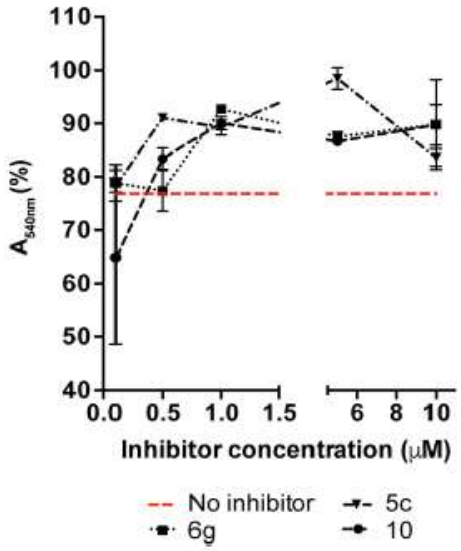

Figure 5

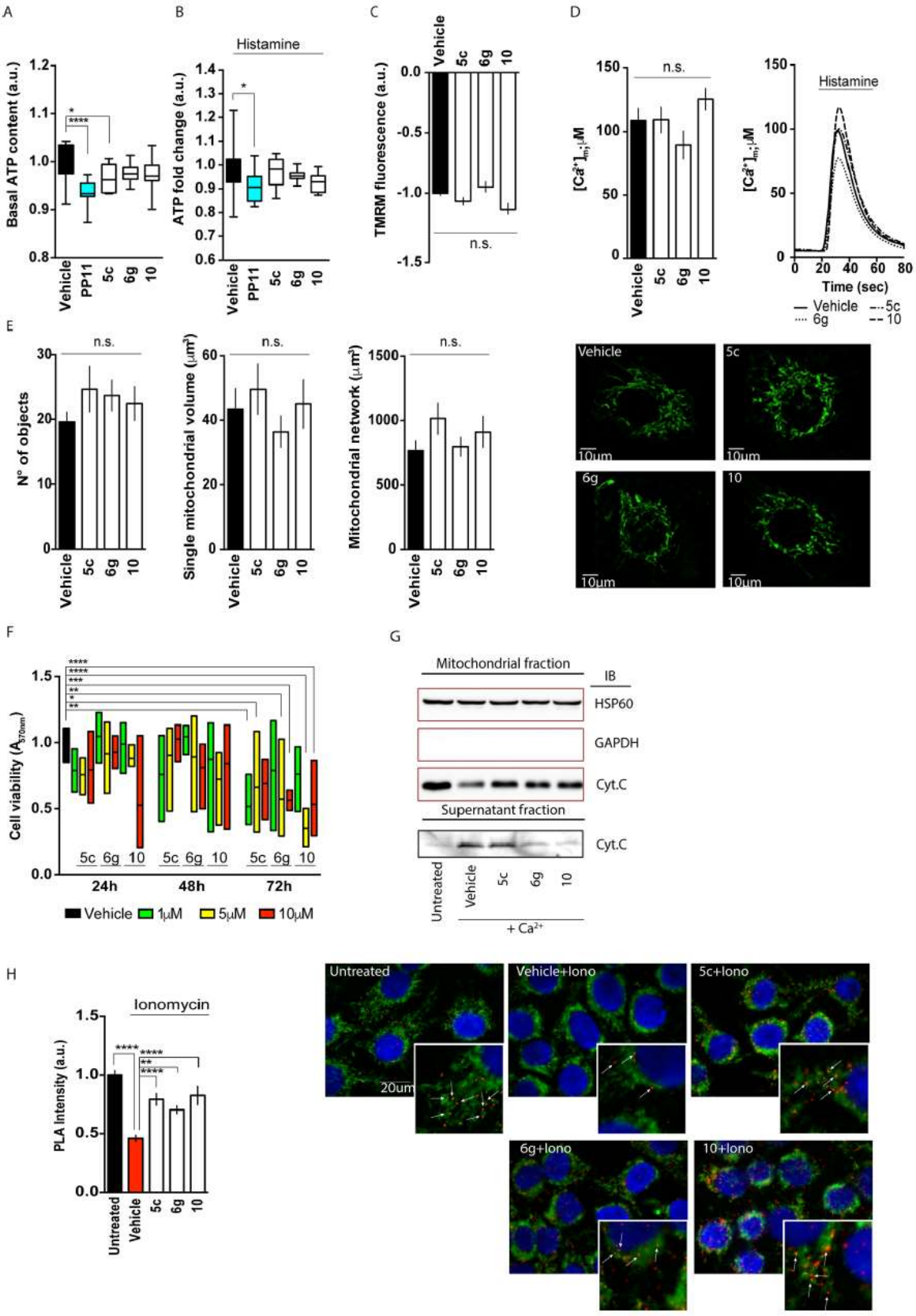
A
Basal ATP content (a.u.)
Vehicle
PP11
5c
6g
10
B
Histamine
ATP fold change (a.u.)
C
TMRM fluorescence (a.u.)
n.s.
D
n.s.
Histamine
Time (sec)
Vehicle
5c
6g
10
E
N° of objects
Single mitochondrial volume (μm³)
Mitochondrial network (μm³)
10μm
F
Cell viability
24h
48h
72h
Vehicle
1μM
5μM
10μM
G
Mitochondrial fraction
IB
HSP60
GAPDH
Cyt.C
Supernatant fraction
Untreated
+ Ca2+
H
Ionomycin
PLA Intensity (a.u.)
Untreated
Vehicle+Iono
5c+Iono
6g+Iono
10+Iono
20um

Figure 6

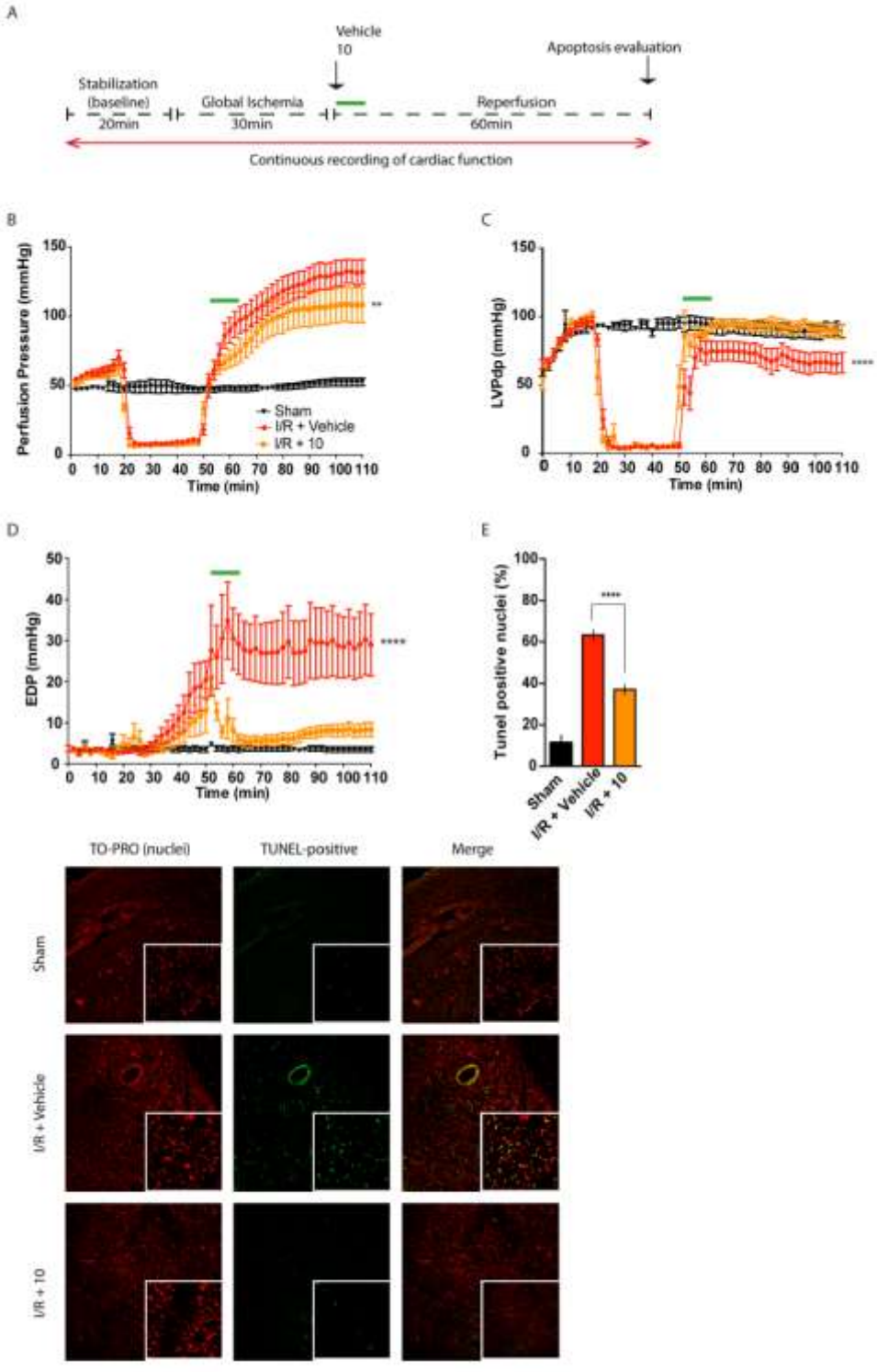
A
Vehicle
10
Apoptosis evaluation
Stabilization
(baseline)
20min
Global Ischemia
30min
Reperfusion
60min
Continuous recording of cardiac function
B
Perfusion Pressure (mmHg)
Time (min)
Sham
I/R + Vehicle
I/R + 10
C
LVPdp (mmHg)
Time (min)
D
EDP (mmHg)
Time (min)
E
Tunel positive nuclei (%)
Sham
I/R + Vehicle
I/R + 10
TO-PRO (nuclei)
TUNEL-positive
Merge
Sham
I/R + Vehicle
I/R + 10

For Table of Contents Only